Optical Probe for Anomalous Hall Resonance in Ferromagnets with Spin Chirality

S. Iguchi,[1] S. Kumakura,[1] Y. Onose,[1,2] S. Bordács,[2,3] I. Kézsmárki,[2,3] N. Nagaosa,[1,4] and Y. Tokura[1,2,4]

[1]*Department of Applied Physics, University of Tokyo, Tokyo 113-8656, Japan*
[2]*Multiferroics Project, ERATO, Japan Science and Technology Agency (JST), Wako, 351-0198, Japan*
[3]*Condensed Matter Research Group of the Hungarian Academy of Science and Department of Physics, Budapest University of Technology and Economics, 1111 Budapest, Hungary*
[4]*Cross-Correlated Materials Research Group (CMRG), ASI, RIKEN, Wako 351-0198, Japan*

(Received 1 August 2009; published 31 December 2009)

We have investigated the infrared optical Hall conductivity, $\sigma_{xy}(\omega)$ for band-filling-controlled ferromagnetic crystals of $Nd_2Mo_2O_7$, revealing the dynamical properties of their anomalous Hall effect (AHE). A resonant structure and its systematic filling dependence were observed in the Hall conductivity spectra in the midinfrared region (typically at 0.1 eV), while similar effects were not discerned in the diagonal (longitudinal or ordinary) conductivity spectra. This property of $\sigma_{xy}(\omega)$ provides crucial and essential information to understand the microscopic mechanism of AHE including its dc limit. Specifically, the interband transition at the magnetic-monopole-like band-anticrossing point, which is split by spin chirality, is the dominant source in AHE.

DOI: 10.1103/PhysRevLett.103.267206 PACS numbers: 78.20.Ls, 75.47.−m, 78.20.Bh

The Hall effect in matter is a general consequence of broken time-reversal symmetry [1]. This phenomenon is enhanced in ferromagnets by the interplay of the spin-orbit interaction and the exchange splitting and is termed the anomalous Hall effect (AHE) [2]. A deep understanding of the underlying physics has been motivated by the discoveries of the integer and fractional quantum Hall effects [3,4] and the spin Hall effect [5]. Long before the discovery of the dc Hall effect, Faraday observed the rotation of the plane of polarization for visible light propagating through transparent magnetic media [6]. This was followed by the detection of magnetic circular dichroism and birefringence over the whole electromagnetic spectrum from radio frequencies to x-ray photon energies.

To be specific, the polar magneto-optical Kerr effect (MOKE) of a ferromagnet—which is the change in the light polarization upon normal-incidence reflection from a surface normal to $\vec{M}$—is described by the off-diagonal elements, $\tilde{\sigma}_{xy}(\omega)$, of the frequency-dependent conductivity tensor. The dc AHE can be understood as the $\omega \rightarrow 0$ limit of this optical response function. Nevertheless, these two effects have been studied and discussed rather separately and the connection between them has seldom been studied systematically. This is partly because MOKE spectroscopy has been used mainly to probe higher energy interband transitions for which the spin-orbit interaction can be treated as perturbation [7]; in contrast, the AHE is sensitive to the fine details of the band structure near the Fermi energy, often appearing as a nonmonotonous function of M [8]. Another reason is the experimental difficulty in performing low-energy (infrared) MOKE spectroscopy, which otherwise could provide a direct connection to the dc AHE. The unique efficiency of broadband magneto-optical spectroscopy to reveal the spin polarized band structure of magnetic materials has recently been applied to itinerant magnets [9–11] and magnetic semiconductors [12,13]. Furthermore, it was used in high-T_c cuprates to confirm the presence of Fermi pockets in the pseudogap state [14].

The intrinsic AHE first proposed by Karplus and Luttinger [15] has recently been formulated in terms of the Berry phase [16]. Beyond the dc Hall effect, this concept has been effectively applied to reproduce the frequency dependence of the off-diagonal conductivity spectrum of magnetic materials such as bcc iron [17]. In the Berry-phase scenario, a band-anticrossing point acts as a magnetic monopole in k space in the presence of the spin-orbit interaction [18], and the induced AHE is expected to show a resonance when the Fermi level lies close to the band-anticrossing point [19,20].

It has been shown that spin chirality also produces the Berry phase and resonant structure [21]. An advantage of the spin-chirality-induced AHE is that the energy scale for the resonant structure is larger than that due to the spin-orbit interaction. The former is related to the tilting angle of the spins and can be of the order of 0.1 eV, while the typical spin-orbit interaction energy is of the order of 20–30 meV for $3d$ transition metal ions. Therefore, we expect the structure of the dynamical $\sigma_{xy}(\omega)$ should be more easily analyzed in the former case. However, the physical picture obtained below applies to the whole class of AHE including those due to spin-orbit interaction as the existence of the band-anticrossing point, not its origin, is crucial for the emergence of the intrinsic AHE.

The pyrochlore metallic ferromagnets $Nd_2Mo_2O_7$ [8,22] and $Pr_2Ir_2O_7$ [23] are unique systems showing noncoplanar spin configuration with (scalar) spin chirality $\vec{S}_i \cdot (\vec{S}_j \times \vec{S}_k)$ formed by neighboring spin sites (i, j, and k). As shown in Figs. 1(a) and 1(b), Nd and Mo spins on the two pyrochlore sublattices of $Nd_2Mo_2O_7$ have Ising- and Heisenberg-like

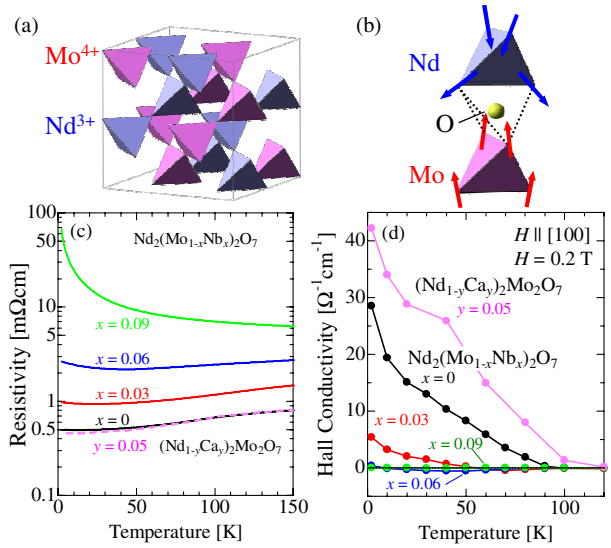

FIG. 1 (color online). (a) Crystal structure of pyrochlore type $Nd_2Mo_2O_7$ and (b) schematic configuration of the Nd and Mo spins. Temperature dependence of (c) resistivity and (d) Hall conductivity in a magnetic field of 0.2 T applied along [100] for $Nd_2(Mo_{1-x}Nb_x)_2O_7$ and $(Nd_{1-y}Ca_y)_2Mo_2O_7$.

character, respectively. The Nd moments exhibit the two-in two-out structure at low temperatures ($\lesssim$30 K); this is similar to spin-ice materials [24]. The Mo moments are aligned ferromagnetically, but slightly canted (by $\sim$1°–4°) via the antiferromagnetic interaction with the Nd moments [8,25]. Itinerant Mo 4*d* electrons in the twofold e_g' orbitals feel the fictitious magnetic field induced by the spin chirality due to the canting of the localized Mo spins in the a_{1g} orbitals. This is expected to be the major origin of the AHE observed for $Nd_2Mo_2O_7$ [8].

Even though the systematic investigation of the AHE by tuning the Fermi level with hole- or electron-doping [18,19,26,27] can be used to search for the resonant effect, a more direct quantity is the ω dependence of $\sigma_{xy}(\omega)$ determined by magneto-optical Kerr spectroscopy [10,28]. The ultimate experimental proof, i.e., the analysis of a resonance in the $\sigma_{xy}(\omega)$ spectra with changes in the doping, has never been achieved so far.

In this Letter, we report a combined experimental and theoretical study of the AHE and infrared MOKE in $Nd_2Mo_2O_7$ and its filling-controlled analogs. It was reported in a previous study [10] that the infrared MOKE signal (above 0.2 eV) or $\sigma_{xy}(\omega)$ is much larger in $Nd_2Mo_2O_7$ than in $Gd_2Mo_2O_7$ with no spin chirality, in accord with their different magnitudes of dc σ_{xy}. Here, by the extended infrared MOKE study ($\gtrsim$0.1 eV) on systematically filling-controlled $Nd_2Mo_2O_7$, we have successfully observed a peak structure in $\sigma_{xy}(\omega)$ at 0.1–0.3 eV, which can be identified as a band-anticrossing point near the Fermi level as playing the dominant role in dc AHE as well. The systematic shift of this resonance and the corresponding change in the AHE was followed by tuning the distance of the anticrossing point from the Fermi energy by doping.

All of the samples used in this study were single crystals grown with a floating-zone furnace in an Ar atmosphere. Figure 1(c) shows the temperature dependence of resistivity in $Nd_2(Mo_{1-x}Nb_x)_2O_7$ (electron doping by Nb^{5+}) and $(Nd_{1-y}Ca_y)_2Mo_2O_7$ (hole doping). While the resistivity is not strongly affected by Ca doping, it increases steeply with Nb doping. This is caused by the doping-induced disorder at Mo sites acting on the itinerant carriers that are responsible for low-energy metallic transport [22]. In Fig. 1(d), we show the temperature and doping dependences of the Hall conductivity with a magnetic field of 0.2 T applied along the [100] easy axis. This field is sufficient to align the magnetic domains along the [100] direction without decreasing the tilting angle of the Mo spins and the corresponding spin chirality. While the Hall conductivity increases with Ca doping, it decreases steeply with Nb doping.

Reflectivity spectra of the crystals were measured at normal incidence to the (100) surface over the energy range of 0.01–5 eV. Their variation with doping at 10 K is shown in Fig. 2(a) on a logarithmic photon-energy scale. Because of the (semi-)metallicity of the specimens, a high-reflectivity band appears below the plasma edge of $\sim$1 eV. Higher energy (4–40 eV) reflectivity spectra measured at room temperature were used to facilitate a Kramers-Kronig

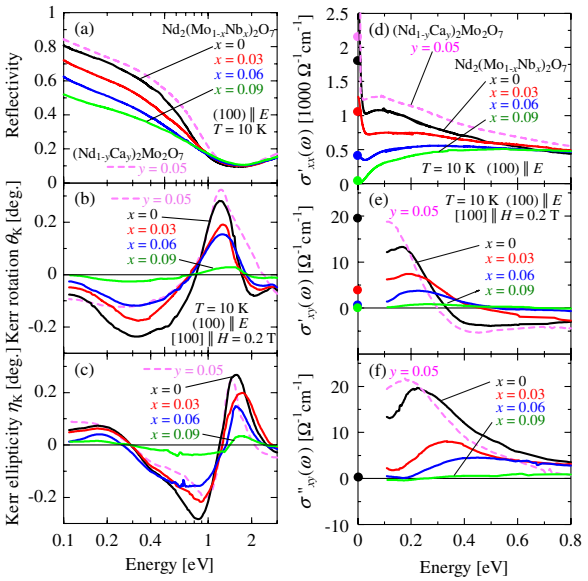

FIG. 2 (color online). The reflectivity (a), Kerr rotation (b), and Kerr ellipticity (c) spectra over the photon-energy range of 0.1–2.5 eV in $Nd_2(Mo_{1-x}Nb_x)_2O_7$ and $(Nd_{1-y}Ca_y)_2Mo_2O_7$ at 10 K. The real part of the diagonal optical conductivity spectra $\sigma_{xx}'(\omega)$, and the real (e) and imaginary (f) parts of the Hall conductivity $\tilde{\sigma}_{xy}(\omega)$ in the infrared region. For $\sigma_{xx}'(\omega)$, the spiky structures due to the optical phonons (0.02–0.06 eV) are removed from the figure for clarity. The dots on the vertical axis indicate the dc values. Note $\sigma_{xy}''(\omega)$ should go to zero in the dc limit by definition.

transformation to obtain the diagonal (longitudinal) optical conductivity, $\tilde{\sigma}_{xx}(\omega)$. Its real part, $\sigma'_{xx}(\omega)$, at 10 K is shown for the Mo 4d intraband region (<0.8 eV) in Fig. 2(d). For the metallic crystals ($x \lesssim 0.03$ and $y = 0.05$), a Drude-like response is observed below 0.05 eV; its $\omega \to 0$ limit corresponds well to the dc conductivity value. On the other hand, the $\sigma'_{xx}(\omega)$ spectra above 0.1 eV are characterized by a broad and nearly frequency-independent structure as is typical for correlated *bad metals* [29]. While the dc conductivity varies over 2 orders of magnitude with Nb doping, the optical conductivity for >0.1 eV shows much less variation with doping. The minimal influence of disorder in this energy range (>0.1 eV) enables us to analyze the effect of band filling on the magneto-optical response, as discussed below.

The spectra of Kerr rotation $\theta_K(\omega)$ and Kerr ellipticity $\eta_K(\omega)$ were measured for the (100) surface of the crystals in a magnetic field of 0.2 T applied normal to the surface (in the polar Kerr configuration) using the polarization-modulation technique [13,30]. Figures 2(b) and 2(c) show the doping variation of $\theta_K(\omega)$ and $\eta_K(\omega)$ spectra at 10 K. The prominent peak in $\theta_K(\omega)$ around 1.2 eV and the dip and peak structures at 0.9 eV and 1.5 eV, respectively, in the $\eta_K(\omega)$ spectra are present for all of the crystals and correspond to the so-called plasma-edge enhancement due to the small value of $|\epsilon'_{xx}(\omega)|$ [31]. The low-energy signals below 0.5 eV are smaller but clearly discerned; these represent the Mo 4d intraband contributions. The optical Hall conductivity $\tilde{\sigma}_{xy}(\omega)$ [Figs. 2(e) and 2(f)] is calculated via the expression [7,31]

$$\tilde{\sigma}_{xy}(\omega) = \sigma'_{xy}(\omega) + i\sigma''_{xy}(\omega) = -[\theta_K(\omega) + i\eta_K(\omega)]\tilde{\sigma}_{xx}(\omega) \times \sqrt{1 + 4\pi i\tilde{\sigma}_{xx}(\omega)/\omega}.$$

The anomaly observed in the Kerr parameters at the plasma edge does not emerge in the Hall conductivity $\tilde{\sigma}_{xy}(\omega)$, which ensures the accuracy of the measurement and analysis. Both the real $[\sigma'_{xy}(\omega)]$ and imaginary $[\sigma''_{xy}(\omega)]$ parts of the Hall conductivity spectra, shown over the midinfrared range in Figs. 2(e) and 2(f), have broad but prominent peaks in contrast to the flat nature of $\sigma'_{xx}(\omega)$. For doping $x \geq 0.03$, the peak in $\sigma'_{xy}(\omega)$ is even larger than the dc value. The peak in the Hall conductivity spectrum systematically shifts to higher and lower energy for electron (Nb) and hole (Ca) doping, respectively, and the broadening of the peak increases for higher peak energies. The energy position of the $\sigma'_{xy}(\omega)$ resonant structure is anticipated to be closely related to the band-anticrossing point (k-space monopole position) beneath the Fermi level, as argued below.

Figure 3(b) shows the hole (y) and electron (x) doping dependencies of the dc anomalous Hall conductivity, σ_{xy}(dc), the peak magnitude of the real part of optical Hall conductivity in the midinfrared (MIR) region, $\sigma'_{xy}(E_{\mathrm{MIR}})$, and the estimated magnetization of Mo spins

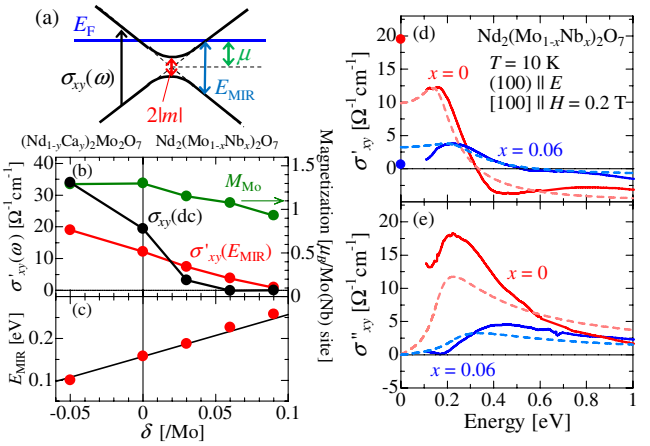

FIG. 3 (color online). (a) The schematic view of the two-band model and its parameters E_F, μ, and m representing the Fermi energy, the distance of the band-anticrossing point from E_F, and half of the energy gap, respectively. (b) Hole (y) and electron (x) doping (band-filling change $\delta = x - y$) dependence of the dc anomalous Hall conductivity σ_{xy}(dc), the peak magnitude of the real part of the optical Hall conductivity in the midinfrared region $\sigma'_{xy}(E_{\mathrm{MIR}})$, and the estimated magnetization of the Mo spin (M_{Mo}) at 10 K. (c) Doping dependence of the peak position E_{MIR} in $\sigma'_{xy}(\omega)$ spectra located in the midinfrared region. The line shows the peak position shift corresponding to the slope E_{MIR}/δ of 1 eV · Mo. Comparison between the experimental spectra (solid lines) and the two-band model calculations (broken lines) for (d) the real and (e) the imaginary part of $\tilde{\sigma}_{xy}(\omega)$ for $x = 0$ and 0.06.

(M_{Mo}). While the M_{Mo} does not show a large filling variation, σ_{xy}(dc) decreases steeply with Nb doping, which is mainly caused by the increase in scattering due to disorder on the Mo (Nb) sites as discussed in Ref. [22]. The midinfrared optical Hall conductivity, $\sigma_{xy}(E_{\mathrm{MIR}})$, also decreases with Nb doping, but the decrease is much weaker than in the dc case. The energy of the band-anticrossing point, if existing to govern the Hall resonance, measured from Fermi energy is expected to increase linearly with the change in filling, $\delta(\simeq x - y)$. To check this, we show the filling dependence of the $\sigma'_{xy}(\omega)$ peak position E_{MIR} in Fig. 3(c) which indeed increases linearly with δ. The slope is comparable with that from the density of states (~1/eV · Mo) obtained by a local-density approximation (LDA) band-structure calculation [32]. The enhancement of the AHE upon hole doping, with little change in resistivity [Fig. 1(c)], is likely due to the redshift of the resonant peak.

To account for the $\tilde{\sigma}_{xy}(\omega)$ resonant spectral shape and its position in terms of the k-space monopole scenario, we consider a two-band Hamiltonian $\mathcal{H} = \Sigma_k C^\dagger(k)H(k)C(k)$. $H(k)$ is expanded as follows: $H(k) = h_0(k)1 + \sum_{i=1}^{3} h_i(k)\sigma_i$, where $C(k) = {}^t[C_{1k}, C_{2k}]$ is the annihilation operator, and $h_i(k)$ and σ_i are the expansion coefficients and the Pauli matrices, respectively. We take $h_0 = -\mu$ (the energy difference between E_F and the band-anticrossing point), $h_1 = \hbar k_x$, $h_2 = \hbar k_y$, and $h_3 = m$ as a

simple two-dimensional model, which describes the enhanced contribution to $\tilde{\sigma}_{xy}(\omega)$ due to the rapid change of the wave function in the momentum space. The energy dispersion is depicted in Fig. 3(a) with the band gap being $2|m|$. The frequency-dependent transverse (off-diagonal) conductivity is calculated with the Kubo formula with the current operator $J_\nu = \frac{e}{\hbar}\sum_k C^\dagger(k)\frac{\partial H(k)}{\partial k_\nu}C(k)$. Then, the explicit $\tilde{\sigma}_{xy}(\omega)$ at 0 K can be calculated by integrating over the 2D k space. The three dimensionality gives the k_z dependence of the mass m, which we take into account approximately by replacing ω by $\omega + i/\tau$ with $1/\tau$ being the broadening factor due to the distribution of m:

$$\tilde{\sigma}_{xy}(\omega) = \frac{e^2}{8\pi h a}\frac{m}{(\hbar\omega + i\hbar/\tau)}\ln\left(\frac{-\hbar\omega - i\hbar/\tau + 2\mu}{\hbar\omega + i\hbar/\tau + 2\mu}\right).$$

Here, a is the interlayer spacing in this quasi-2D model, corresponding to the lattice constant (~1 nm) [33].

The results of fitting the experimental spectra with this formula are shown by the broken lines in Figs. 3(d) and 3(e). The parameters of μ, $\hbar/\tau$, and m obtained by the fitting are 78, 40, and 78 meV for $x = 0$ and 113, 80, and 41 meV for $x = 0.06$, respectively. The present simple model calculation can well capture the observed features; the peak energy in the imaginary part positions higher than that of the real part and the peak magnitude decreases with increasing the peak position ($\propto m/\omega$). The difference between the $\omega \to 0$ limit of $\sigma'_{xy}(\omega)$ and the observed $\sigma_{xy}(\mathrm{dc})$ is considered as the contribution from the experimentally inaccessible low-energy band structure. The interband transition peak is expected to locate at $E_p \simeq 2\mu$ in the present model. Therefore, the peak position shift per δ $(\frac{\partial E_p}{\partial \delta})$ is expected to be $\frac{2}{D(\epsilon_F)}$. The experimentally observed $\frac{\partial E_p}{\partial \delta}$ gives the value of $D(\epsilon_F) = 2/\mathrm{eV}\cdot\mathrm{Mo}$; this is to be compared with $D_{\mathrm{LDA}}(\epsilon_F) \sim 1/\mathrm{eV}\cdot\mathrm{Mo}$ obtained by the LDA calculation. The discrepancy, i.e., a factor of 2, is viewed as small, considering that the LDA tends to underestimate $D(\epsilon_F)$ due to insufficient correction for the electron correlation; this is manifested by the observed enhancement of the electronic specific-heat coefficient γ as compared with the LDA calculation [34]. The $\sigma'_{xy}(E_{\mathrm{MIR}})$ scales with the band gap $2|m|$ or interaction energy. The obtained m is as large as 80 meV, although the value should be taken as semiquantitive because of the crudeness of the 2D model. Since the dc AHE in $Nd_2Mo_2O_7$ is dominated by the spin chirality rather than the spin-orbit interaction for Mo $4d$ electrons, the presently deduced energy gap at the band-anticrossing point should also stem from the spin chirality.

In conclusion, we have observed a resonant structure in the midinfrared region of the optical Hall conductivity spectra and its systematic evolution in the band-filling-controlled $Nd_2Mo_2O_7$ endowed with spin chirality. The resonant structure is related to the k-space band-anticrossing point associated with a gap induced by the spin chirality. The present result provides the compelling evidence for the monopolelike resonant structure in the k space as expected from the Berry-phase mechanism of the AHE. This picture should generally apply to the whole class of AHE, and the related resonance in the optical Hall conductivity is expected to also be observable if the spin-orbit interaction is sufficiently large for the itinerant ferromagnet.

We thank S. Onoda for helpful discussions. This work was partly supported by KAKENHI (No. 20740186, No. 20340086, No. 20046004, No. 19048015, No. 19048008, No. 21244053, and No. 17105002), MEXT of Japan, , and by the Hungarian Research Funds OTKA PD75615, NK72916, and Bolyai 00256/08/11.

[1] E. H. Hall, Am. J. Math. **2**, 287 (1879).
[2] A. Kundt, Wied. Ann. **49**, 257 (1893).
[3] K. von Klitzing, G. Dorda, and M. Pepper, Phys. Rev. Lett. **45**, 494 (1980).
[4] D. C. Tsui, H. L. Stormer, and A. C. Gossard, Phys. Rev. Lett. **48**, 1559 (1982); R. B. Laughlin, Phys. Rev. Lett. **50**, 1395 (1983).
[5] J. Wunderlich *et al.*, Phys. Rev. Lett. **94**, 047204 (2005).
[6] M. Faraday, Phil. Trans. R. Soc. London **136**, 1 (1846).
[7] P. N. Argyres, Phys. Rev. **97**, 334 (1955).
[8] Y. Taguchi *et al.*, Science **291**, 2573 (2001).
[9] M.-H. Kim *et al.*, Phys. Rev. B **75**, 214416 (2007).
[10] I. Kézsmárki *et al.*, Phys. Rev. B **72**, 094427 (2005).
[11] S. Bordács *et al.*, arXiv:0907.5087.
[12] R. Lang *et al.*, Phys. Rev. B **72**, 024430 (2005).
[13] K. Ohgushi *et al.*, J. Phys. Soc. Jpn. **77**, 034713 (2008).
[14] A. Zimmers *et al.*, Phys. Rev. B **76**, 064515 (2007); L. B. Rigal *et al.*, Phys. Rev. Lett. **93**, 137002 (2004).
[15] R. Karplus and J. M. Luttinger, Phys. Rev. **95**, 1154 (1954).
[16] N. Nagaosa *et al.*, arXiv:0904.4154 [Rev. Mod. Phys. (to be published)]; N. Nagaosa, J. Phys. Soc. Jpn. **75**, 042001 (2006).
[17] Y. Yao *et al.*, Phys. Rev. Lett. **92**, 037204 (2004).
[18] Z. Fang *et al.*, Science **302**, 92 (2003).
[19] M. Onoda and N. Nagaosa, J. Phys. Soc. Jpn. **71**, 19 (2002).
[20] T. Tanaka and H. Kontani, Phys. Rev. B **77**, 195129 (2008).
[21] K. Ohgushi, S. Murakami, and N. Nagaosa, Phys. Rev. B **62**, R6065 (2000).
[22] S. Iguchi, N. Hanasaki, and Y. Tokura, Phys. Rev. Lett. **99**, 077202 (2007).
[23] Y. Machida *et al.*, Phys. Rev. Lett. **98**, 057203 (2007).
[24] S. T. Bramwell and M. J. Gingras, Science **294**, 1495 (2001).
[25] Y. Yasui *et al.*, J. Phys. Soc. Jpn. **72**, 865 (2003).
[26] Y. Yao *et al.*, Phys. Rev. B **75**, 020401(R) (2007).
[27] W.-L. Lee *et al.*, Science **303**, 1647 (2004).
[28] M. C. Langner *et al.*, Phys. Rev. Lett. **102**, 177601 (2009).
[29] M. Imada, A. Fujimori, and Y. Tokura, Rev. Mod. Phys. **70**, 1039 (1998).
[30] K. Sato, Jpn. J. Appl. Phys. **20**, 2403 (1981).
[31] H. Feil and C. Haas, Phys. Rev. Lett. **58**, 65 (1987).
[32] I. V. Solovyev, Phys. Rev. B **67**, 174406 (2003).
[33] Y. Moritomo *et al.*, Phys. Rev. B **63**, 144425 (2001).
[34] N. Hanasaki *et al.*, Phys. Rev. Lett. **99**, 086401 (2007).